PCCP

Accepted Manuscript

This is an *Accepted Manuscript*, which has been through the Royal Society of Chemistry peer review process and has been accepted for publication.

Accepted Manuscripts are published online shortly after acceptance, before technical editing, formatting and proof reading. Using this free service, authors can make their results available to the community, in citable form, before we publish the edited article. We will replace this *Accepted Manuscript* with the edited and formatted *Advance Article* as soon as it is available.

You can find more information about *Accepted Manuscripts* in the Information for Authors.

Please note that technical editing may introduce minor changes to the text and/or graphics, which may alter content. The journal's standard Terms & Conditions and the Ethical guidelines still apply. In no event shall the Royal Society of Chemistry be held responsible for any errors or omissions in this *Accepted Manuscript* or any consequences arising from the use of any information it contains.

ROYAL SOCIETY OF CHEMISTRY

www.rsc.org/pccp

Significant evidence of C⋯O and C⋯C long-range contacts in several heterodimeric

complexes of CO with CH$_3$–X, should one refer to them as carbon- and dicarbon-bonds!

Pradeep R. Varadwaj,[1] Arpita Varadwaj, Bih-Yaw Jin

Department of Chemistry, National Taiwan University, Taipei, 10617, Taiwan

Abstract:

Noncovalent interactions in 18 weakly-bound binary complexes formed between either of the two end-on orientations of the CO molecule and the methylated carbon positive σ–hole associated with the hydrophobic part of the CH$_3$–X molecules are exploited using Density Functional Theory to examine the physical chemistry of 'carbon bonds' recently introduced (Phys. Chem. Chem. Phys. 2013, 15, 14377), where X = –NO$_2$, –CN, –F, –Cl, –Br, –OH, –CF$_3$, –CCl$_3$, and –NH$_2$. The two important types of interactions, C⋯O and C⋯C, the latter never exploited before, identified are found to be stabilized by charge transfer delocalizations between the electron-acceptor and -donor natural bond orbitals of the interacting partners involved, unveiled using natural bond orbital analysis. Application of atoms in molecules theory revealed preferable quantum mechanical exchange-correlation energy channels, and (3, −1) bond critical points (bcps), between the atoms of noncovalently bonded pairs in these complexes, in excellent agreement with the results of the NonCovalent-Interaction Reduced-Density-Gradient (NCI-RDG) theory that revealed expected isosurfaces and troughs in the low density region in the RDG vs. sign(λ_2)ρ plots. The dependencies of the C⋯O and C⋯C bcp charge densities on their corresponding local energy densities, as well as that on their corresponding bond electron delocalization indices, are found to show the nontrivial role of these topological descriptors to explain the stabilities of the binary complexes investigated. Besides, the vibrational red- and blue-shifts in the CO bond stretching frequencies, together with concomitant elongations and contractions of the corresponding bond lengths, both with respect to the monomer values, are observed upon formation of the C⋯O and C⋯C bonded complexes, respectively. The increase and decrease in the complex dipole moments, relative to the sum of their respective monomer values, are found to be a characteristic that separates the red- and blue-shifted interactions mentioned just above. In analogy with dihydrogen bonding, as well as that with the charge and electrostatic potential model descriptions, we suggest the C⋯C interactions to be referred to as dicarbon bonds.

[1] Corresponding Author's Email Addresses: pradeep@t.okayama-uc.jp (PRV), byjin@ntu.edu.tw (BYJ)

Tel: +886-2-33661165, Fax: +886-2-23636359

1.   Introduction

Owing to their application diversity in many areas of science, the chemistry of noncovalent interactions is expeditiously growing in the last five years.[1-2] These least understood chemical interactions came into sight since Pauling gave a formal definition to hydrogen bond in 1939,[3] viable not only for the rapid development of biomolecular drugs and supramolecular assemblies, but also for the rationale design of novel materials for applications in nano- and bio-sciences.[2]

Noncovalent interactions are either intramolecular or intermolecular depending on whether the long-range force operating between the two adjacent atoms is existing within a molecule or between two separate molecules. In the literature, these interactions are exemplified with varieties of names, such as the van der Waals,[4] hydrogen bond,[5-6] dihydrogen bond,[7-8] chalcogen bond,[9-10] pnictogen bond,[5,9-10] σ-hole bond,[8,11] halogen bond,[1,8,11] carbon bond,[12] and tetrel bond[13] etc., with each is having chemical, physical, and spectroscopic properties similar to, or differ from, the other.

We are interested in the study of noncovalent interactions, specifically those involving the least explored group 14 elements. An initial work on these was first reported by Bundhun and coworkers,[14] wherein the nucleophillic nitrogen center was linked collinearly with the electrophillic carbon σ-hole in CF_3–X leading to the formation of the $HCN \cdots MF_3$–X (X = F, Cl, Br, I; M = C, Si, Ge,) complexes. Since then a number of theoretical studies on these interactions are reported.[12,13,15-23] For instance, in 2013, Mani et al reported using first-principles methods the geometrical, vibrational, and topological charge density properties of the $D \cdots CH_3$–X complex series, where X = OH, F, Cl, Br, NH_2, NO_2, and NF_2, and D is covalently bonded to the atom Y, with D = O, S, F, Cl, Br, N, and P.[12] They tried addressing in that study whether the specific interaction appearing between the hydrophobic part of the CH_3–X subunits and a series of electron donors in the complexes has something to do with hydrophobic interaction widely recognized in biology. In analogy with halogen bonds,[1,2,8,11] they introduced term 'carbon bond' to recognize the $D \cdots C$ interaction, and suggested treating a part of the hydrophobic interaction as carbon bond.[12,15]

Later on, the term 'tetrel bond' was introduced by some authors to cover all group 14 elements having noncovalent interactions.[15-17] In most of these above studies, the main focus of research was on the fundamental understanding and importance of these bonds in S_N2 reactions,[12,15-17] and in σ-hole bonding,[18-20] as well as in the design of anion receptor hosts.[21-22] For instance, Grabowski showed in a recent study that the formation of tetrel bond is often a preliminary stage of the S_N2 reaction, in which, a

nucleophile upon it reaction with the sp^3–carbon center in CH_3–X, leading to the loss of the electronegative leaving group X with inversion of stereochemistry.[16] Similarly, Azofra and coworkers showed using Density Functional Theory (DFT) calculations that analogous carbon bonded interactions are abundantly present in the carbohydrates as stabilizing forces in the form of $O\cdots C(sp^3)$, such as in the open-chain forms of both the monosaccharides and the α- and β-furanose configurations of 2-deoxy-D-ribose, as well as in open-chain D-ribose (e.g., α-2-deoxy-D-ribofuranose, and β-2-deoxy-D-ribofuranose).[22] The genuinely of carbon bonds are enlightened early this year by X-ray crystallographic measurements, transpired in a number of heterodimers.[23]

Considering the importance of the carbon bonds discussed just above, as well as the fact that they play a crucial role in the stabilization of the intermediates in the S_N2 reactions,[12,14-23] one may readily pose the question: whether can one, in a manner similar to how the carbon bond was introduced,[12] transmit the concepts of dihydrogen (H$\cdots$H) bonding[7-8] to dicarbon (C$\cdots$C) bonding for their easy reorganization? In an attempt to answer this very important question, the electronic structures of eighteen heterodimeric complexes are thoroughly explored using Density Functional Theory[24] with PBE0,[25] in combination with Quantum Theory of Atoms in Molecules (QTAIM),[26-27] Natural Bond Orbital (NBO),[28-30] Molecular Electrostatic Surface Potential (MESP),[8,11] and Non-Covalent Interaction (NCI) Reduced-Density-Gradient (RDG) plot analyses.[31-32] The dimeric complexes considered in this study are expected to be formed by linking monomers of two different varieties, one the carbon monoxide (CO) molecule and one CH_3–X series of nine molecules, where X = $-NO_2$, $-CN$, $-F$, $-Cl$, $-Br$, $-OH$, $-CF_3$, $-CCl_3$, and $-NH_2$. We address in this paper, among other things, the following questions:

(i) Because the CO molecule is having two local most negative areas of electrostatic potential, one on a given atom, on the outermost extension of its covalent bond,[33] can one expect any long range contact when each of these two negative areas of electrostatic potential is to be exposed with the positive area of electrostatic potential localized on the carbon surfaces of the CH_3–X molecules, on the extensions of the X–C covalent bonds?

(ii) How, and to what extent, the varying nature of the substituents X in CH_3–X would influence the 1:1 coordination mode, the polarity, the charge distribution, and the binding energy of the resulting YD$\cdots CH_3$–X (D = CO, OC) binary complexes at their equilibrium static geometries.

(iii) Given there is some controversy associated with the determination of atomic charges,[8,17,13,34] would it still be physically meaningful to use atomic charges to determine the nature of charge-

redistribution and -transfer effects that accompany complex formation; these features are previously studied for numerous intermolecular complexes.[12,13,15,16,35-39]

(iv) Can we expect a reasonable consistency between the physical properties of the D···CH$_3$–X (D = CO, OC) complexes to be emerged from the various theoretical approaches employed (such as those from to be emerged from the NBO, QTAIM, NCI-RDG, and MESP methods)? This was recently debated,[40] wherein it was vividly shown that the QTAIM controversially rejects some systems which are otherwise appeared to be noncovalently bonded.

(v) Can one expect dependencies between the bond electron delocalization indices and bond critical point (bcp) charge densities, as well as of the former and the intermolecular bond distances for the O···C and C···C interactions to be emerged; these sorts of relationships are previously recognized for covalently- and H-bonded systems explaining complex stabilities.[41-44]

2.   Results and discussion

2.1   Electrostatic surface potentials of monomers

Figure 1 illustrates the AIMALL[45] generated molecular graphs for some selected geometries of the monomers; Gaussian 09[46] was used to energy-minimize these geometries. The MESP analyses were carried out using MultiWfn,[47] this was performed for all the monomer geometries to identify the reactive sites, and to evaluate the local most maxima and minima values of electrostatic potential on their surfaces ($V_{s,max}$ and $V_{s,min}$, respectively); a detail on this is given in the Electronic Supporting Information (ESI). **Figure 2,** for example, depicts the 0.001 au mapped MESP graphs for three randomly selected species that include CH$_3$–Cl$_3$, CH$_3$–F and CO, showing the regions electrophillic and nucleophillic attacks.

Of interest is the local most electrophillic areas of electrostatic potential on the surfaces of the methylated carbon in CH$_3$–X on extensions of the X–C bonds. These are calculated to be +28.61, +23.43, +20.89, +17.40, +16.17, +10.58, +17.34, +16.36, and +3.31 kcal mol^{-1} for CH$_3$–NO$_2$, CH$_3$–CN, CH$_3$–F, CH$_3$–Cl, CH$_3$–Br, CH$_3$–OH, CH$_3$–CF$_3$, CH$_3$–Cl$_3$, and CH$_3$–NH$_2$, respectively. Perhaps, the decreasing nature of the carbon's $V_{s,max}$ in the series displays the preferred electron withdrawing abilities of the nine substituents.

As clarified in Figure 2c, we traced no positive regions of electrostatic potential on the atomic surfaces of the CO molecule on the extension of its covalent bond. This is rather confined in the central bonding region as a blue cylinder ($V_{s,max}$= +12.31 kcal mol^{-1}). The corresponding $V_{s,min}$ are ca. −7.09 and

−12.76 kcal mol^{-1}, localized on the outermost surfaces of the oxygen and carbon atoms on the extension of the CO bond, respectively. The results are in agreement with the M06–2X/6-311G(d) data of Murray and Politzer ($V_{s,min}(O)$ = −8.4 kcal mol^{-1} and $V_{s,min}(C)$ = −12.5 kcal mol^{-1}).[33] The small difference between the $V_{s,min}$ values of this work and of Murray et al can be attributed to the two computational methods by which they are obtained. The above results suggest that the carbon's lone pair negative potential, compared to that on the oxygen atom, in CO may be more reactive so as to act as an efficient electron donor for the methylated carbon σ–hole in CH$_3$–X.

2.2   Geometrical stabilities of binary complexes

Given a σ–hole donor molecule, the two energy-minimized geometries resulted are a O···C bonded, and a C···C bonded, appeared due to the two end-on orientations of the CO species (see, Figures 3(a) and 4(a), as examples). In each case, the nucleophile (O or C end lone pair electrons of CO) attacks in a direction opposite to the X–C bond. Without the loss of generality, these results compel one to admit that the outcome is actually similar to what happens in the primary stage of a S$_N$2 reaction during an intermediate formation, in which, the sp^3 aliphatic carbon within its first coordination sphere is being five-coordinate, forming with the main group atoms two pairs of four short covalent bonds, and a very long bond (electrostatically stabilized?).

The geometries of the D···CH$_3$–X (D = CO, OC) complexes yielded each is a local minimum on its potential energy surface, except for Figure 4g. This latter complex is apparently a second order transition point TS2, confirmed by the analytical Hessian calculation (the two negative (imaginary) frequencies are −18.0 and −17.0 cm^{-1}).

The $r(O···C)$ bond distances of separation between the monomers in CO···CH$_3$–X are lying between 3.350 and 3.748 Å. In contrary, the $r(C···C)$ bond distances in OC···CH$_3$–X are between 3.516 and 3.811 Å (see **Table 1** for details). Notably, most of the intermolecular bond distances in the former complexes each is less than the sum of the van der Waals radii of the bonded atoms, vdW$_{O+C}$ and rVdW$_{C+C}$, where rvdW(C) = 1.77 Å, and rvdw(O) = 1.50 Å.[48] However, an opposite feature is encountered for most of the bond distances in the latter complexes. This is may be trivial as the two carbon atoms in the C···C bonded pairs display their competence to govern very long-range intermolecular contacts. Mani and Arunan previously reported a comparable range of values for F···C, N···C, P···C, O···C, Cl···C, and S···C contacts (e.g., 2.985 – 3.803 Å with MP2).[12]

The three consecutive atoms involved in the intermolecular bonded pairs in most of the CO⋯CH$_3$–X and OC⋯CH$_3$–X geometries are nearly collinear. This is evident of the angles, $\angle$C=O⋯C and $\angle$O=C⋯C, which are close to 178 – 180°, reflecting the directional nature of the methylated carbon σ–hole in CH$_3$–X. An exception to this bond angle range is found for OC⋯CH$_3$–OH, CO⋯CH$_3$-NH$_2$ and OC⋯CH$_3$-NH$_2$ (see Figures 4f, 3e and 4e, respectively). For instance, the O=C⋯C (C⋯C–X) angles in these three complexes are ca. 161.0 (178.9), 175.1 (177.1), and 143.9 (173.7^o), respectively, implying that the intermolecular angular geometries in these complexes are largely distorted. The very large geometrical distortion in OC⋯CH$_3$-NH$_2$ is due to the presence of a secondary interaction, which is occurring between the carbon end of CO and the mid-point of a C–H bond in CH$_3$-NH$_2$ for which there is a curved bond path appearing between them. This result can be comparable with what was previously reported for an analogous system,[33] in which case, a deviation of 21° from 180° was noted for halogen bonded $\angle$C–Cl⋯O in the Cl–C(O)-C(O)–Cl⋯1,4-dioxane complex, where there was an involvement of a secondary interaction leading to the hydrogen bond formation. In the other two complexes, OC⋯CH$_3$–OH and CO⋯CH$_3$-NH$_2$, there is no secondary interactions involved between the interacting molecule pairs, the angular distortion may be (directionally) related to the oxygen and nitrogen lone pair electrons of the substituents, respectively.

2.3   QTAIM based charge density topologies

Whether the O⋯C and C⋯C contact distances discussed above can be considered or not as having noncovalent character are yet unclear. In an effort to shade some light on this, we applied the very popular QTAIM methodology[26-27] to evaluate the topological critical point properties of the charge density for the intermolecular frameworks. **Figures 3 and 4** illustrate the QTAIM molecular graphs for most of the complexes. The intermolecular region in each of these complexes is associated with a (3,–1) bcp and a bond path between CO and CH$_3$–X, typical for closed-shell interactions.[26-27,35,49-50]

The sum of the topological radii r_a+r_b for each pair of two noncovalently bonded atoms listed in Table 2 is equal to its corresponding bond path length r_{bpl}. However, the r_{bpl} values are slightly larger than their corresponding geometrical bond lengths r (Table 1), indicative of strained bonds.[51]

The calculated charge density ρ_b values for the O⋯C bcps are very small, ranging between 0.0018 and 0.0029 au. The Laplacian of the charge density $\nabla^2\rho_b$ for the corresponding bonds are small too, but are positive in signs ($\nabla^2\rho_b > 0$), values varying between +0.0088 and +0.0143 au. These are

physically close to the ρ_b and $\nabla^2\rho_b$ values of 0.0021 − 0.0034 and 0.0076 − 0.0136 au for the C···C bcps, respectively. For comparison, Mani and Arunan reported ρ_b and $\nabla^2\rho_b$ values of 0.0035 - 0.0081 and 0.0140 - 0.0459 au for D···C bcps, respectively, where D = O, S, F, Cl, Br, N, and P.[12] By contrast, the ρ_b values for covalently bonded atom pairs are orders of magnitude larger, see Figure 1 for details.

The local potential energy densities V_b are very small and negative ($V_b < 0$) at the O···C and C···C bcps. These are smaller than the local kinetic energy densities G_b calculated for the corresponding bcps (i.e., $V_b < G_b$). Because of these, one can see from Table 2 that the resulting total energy densities (H_b) are also small and positive at the above bcps, where $H_b = V_b + G_b$. In summary, the results all above are in line with the connotations of Bader,[26] Matta and Boyd,[27] and others,[6,35,41-44,52-54] who have suggested that the positive signs accompanied with $\nabla^2\rho_b$ and H_b ($\nabla^2\rho_b > 0$ and $H_b > 0$), and the very low ρ_b values, are the genuine descriptors of charge depleted intermolecular regions at bcps, which are indeed expected of closed-shell interactions.

Figure 5 displays the contour maps of the $\nabla^2\rho_b$ for some selected monomers and complexes. **Figure 6** shows the relief maps of the $\nabla^2\rho_b$ for two selected heterodimeric complexes. Each of the above graphs elucidates the localized regions of valence charge concentration and depletion required for the formation of noncovalent bonds.[55] Encouragingly, the methylated carbon σ–holes in the monomers discussed in 2.1 above are evident of the $\nabla^2\rho_b$ maps, on extensions of the C–C and Br–C covalent bonds (**Figures 5 and 6**), demonstrating a close resemblance between QTAIM and MESP.

2.4   NCI-RDG plot analysis

The QTAIM criteria proposed by Bader,[27] that is, $\nabla^2\rho_b > 0$ and $\nabla^2\rho_b < 0$, as well as that by others (e.g. the value of the ratio $|V_b|/G_b$ etc.),[42,56] are vastly invoked in the past to identify the opened-shell (covalent, and metal-ligand bonds) and closed-shell (as in ionic bonds, H-bonds, or van der Waals etc.) atom pair contacts in diverse compounds. However, it is just recently argued that the above criteria may not be suitable for the search of a bonding interaction, especially when electron density in the bonding region is very weak (and very flat) in real space.[40] 1,2-ethanediol[40] and 2-fluorophenol[57] are the two examples for which the QTAIM finds no preference for displaying an intramolecular hydrogen bonding interaction, although these two systems were unequivocally identified to be weakly O···H and F···H bonded based on the NCI-RDG plot analysis,[31-32] in agreement with experiment.[57,58] The main reason for the failure lies in the criteria related to the stringent limits, e.g., the reduced density gradient s = 0.0 au

and the sign of the $\nabla^2 \rho_b$ ($\nabla^2 \rho_b = \lambda_1 + \lambda_2 + \lambda_3$), as this latter is determined by the three diagonal eigenvalues $\lambda_{i=1,2,3}$ associated with the three principal curvatures. To give an example, the calculated eigenvalues $\lambda_{i=1,2,3}$ associated with the three principal curvatures of charge density at the O···C bcp are ca. −0.00125, −0.00097 and +0.01463 au for the CO···CH$_3$–NO$_2$ complex, respectively, and their sum results in the $\nabla^2 \rho_b$ value of +0.01240 au at the corresponding bcp.

Although $\nabla^2 \rho_b > 0$ for the O···C and C···C bcps confirms the electrostatic nature of these interactions, it would still be encouraging to see what the NCI criteria of Johnson et al[31] prevail. According to this, the sign of the second curvature λ_2 alone would trustily discriminate bonding interactions ($\lambda_2 < 0$) from non-bonding and steric clashes ($\lambda_2 > 0$). And, because the NCI is solely based on the charge density and its derivatives given by Eq. 1, it therefore recuperates the QTAIM results and provides systematic changes in the reduced density gradient expected of bonding regions, [31-32,40] where ∇ is the nabla operator, ρ is the electron charge density, RDG is the reduced-density-gradient (s).

$$s = \frac{1}{2(3\pi^2)^{1/3}} \frac{|\nabla \rho|}{\rho^{4/3}} \dots\dots\dots\dots\dots\dots\dots\dots\dots\dots\dots\dots\dots\dots\dots\dots\dots(1)$$

The eigenvalues $\lambda_{i=1,2,3}$ associated with the three curvatures of charge density at the C···O and C···C bcps are listed in Table 2. For each of these interactions, $\lambda_{1,2} < 0$, $\lambda_3 > 0$, and $|\lambda_2| < |\lambda_1| < |\lambda_3|$, fitting exactly with the bonding criterion of Johnson et al.[31]

Figure 7 plots RDG (s) against sign(λ_2)ρ for six randomly selected intermolecular complexes, including CO···CH$_3$–CCl$_3$, CO···CH$_3$–Br, and CO···CH$_3$–NH$_2$, and their corresponding C···C bonded analogues. As one sees, there are two spikes corresponding to each of these complexes. One is very sharp, long, and strong, and peaks in the region −0.0015 < sign(λ_2)ρ < −0.0040 au, whereas the other is sharp, short and weak, and peaks in the region 0.002 < sign(λ_2)ρ < 0.004 au. These are centered on either sides of sign(λ_2)ρ = 0.0 au, and are corresponding to the low s and low density regions expected of weakly bonded intermolecular interactions.

The s = 0.5 au RDG isosurfaces are also shown in Figure 7. Each of these isosurfaces represents to a single triangular-shaped volume painted in green in the low density region, appearing between the methylated carbon σ–hole in CH$_3$–X and the donor atom of the CO molecule in the complexes (see the ball and stick models). The triangular-shape can be viewed as consisting of positive contributions from the local sources, such as from the covalently bonded hydrogen atoms of the −CH$_3$ group to the bcp charge densities of the O···C and C···C interactions. These results clearly demonstrate an unambiguous compatibility between QTAIM and NCI-RDG.

2.5   Energetic stabilities

Of significant interest in the study of noncovalent interaction is the evaluation of the complex binding energy, ΔE. This is calculated using Eq. 2, where E on the R. H. S. of Eq. 2 denotes the total electronic energy of the $D \cdots CH_3-X$ (D = CO, OC) complex, and of the monomers in it, and $\sum$ denotes the sum over the two monomers. The ΔE values are listed in Table 1. The data show that, for a given orientation of the CO molecule, the largest and the smallest values of the ΔE are to be associated with the complexes of it with CH_3-NO_2 and CH_3-NH_2, respectively. Encouragingly, this parallels with the strongest and the weakest electron-withdrawing abilities of the respective substituents, $-NO_2$ and $-NH_2$, in CH_3-X in the series, a result which is consistent with their corresponding strengths of the carbon $\sigma-$hole electrostatic surface potential on the these monomers.

$$\Delta E = E(D \cdots CH_3-X) - \sum (E(CO) + E(CH_3-X)) \dots\dots\dots\dots\dots\dots\dots\dots\dots\dots\dots\dots (2)$$

The binding energies collected in Table 1 are all squeezed into a very narrow range between -1.01 and -2.30 kJ mol^{-1} for the $CO \cdots CH_3-X$ complexes, and that between -1.06 and -3.10 kJ mol^{-1} for the $OC \cdots CH_3-X$ complexes. The zero-point vibration slightly affects the ΔE, downshifting them to range between -0.36 and -1.64 kJ mol^{-1} for the former, and that between -0.35 and -2.24 kJ mol^{-1} for the latter complexes, respectively (see Table 1 for the ΔE^{zpe} values). The basis set superposition error (BSSE) accounted for by the counterpoise correction procedure of Boys and Bernardi[61] are estimated to lie between 0.54 and 1.12 kJ mol^{-1} for the whole series of the binary complexes, the largest of which is associated with $OC \cdots CH_3Cl_3$. And, an involvement of the BSSE retains the negative sign of ΔE for the $D \cdots CH_3-X$ complexes.

In order to check the room temperature stabilities of the $D \cdots CH_3-X$ complexes, the binding energies (ΔH) are also estimated with PBE0 at 298.15 K by subtracting the enthalpies of the complexes from the sum of their corresponding monomer values. Except for $OC \cdots CH_3-CCl_3$ (for which $\Delta H < 0$), we found all the other complexes to have positive ΔH (i.e., $\Delta H > 0$), showing a stability reversal, evocative of thermodyanamically unstable structures. Nevertheless, according to Politzer and Murray,[33] and others,[59-60] many complexes of this type which are energetically endothermic in the gas phase are stable in the solution and solid phases.

What is most striking from the ΔE data is that given a σ–donor molecule the C···C interaction is energetically favorable over, or somewhat closer to, the corresponding O···C interaction, i.e., ΔE(C···C) ≥ ΔE (O···C). Whether is this particular effect more general? Or, this is an error of the computational method, asked by a reviewer. We addressed this fundamental question as follows. We reoptimized the geometries of two randomly selected complexes, D···CH_3–X (X = F, D = OC, CO), and their monomers, with a higher level of theory, QCISD(fc)/6–311++G(d,p), where QCISD refers to Quadratic Configuration Interaction calculation including single and double substitutions,[58] and 'fc' in the parenthesis denotes to frozen-core approximation. The binding energies for these two complexes are then calculated using Eq. 2. Not surprisingly, we found this method also predicts a very small difference between the binding energies of the two complexes. For instance, the QCISD binding energies are −3.04 and −3.20 kJ mol^{-1} for OC···CH_3–X and OC···CH_3–X, respectively, and their difference value is 0.16 kJ mol^{-1}. This, together their respective intermolecular distances of separation of 3.2705 and 3.6201 Å, is in qualitative agreement with PBE0.

To insight further into the details of the component energy contributions to the complex interaction energies, Localized Molecular Orbital-Energy Decomposition Analysis (LM-OEDA) tool[78] implemented in Gamess code[79] was employed. Without any specific bias, this analysis was performed only for OC···CH_3–F and CO···CH_3–F on their QCISD(fc) optimized geometries with CCSD/aug-cc-pVTz.[80] The interaction energies thus resulted are −3.43 and −3.89 kJ mol^{-1} for these complexes, respectively, comparable with QCISD. And, an inspection of the individual component energy values of −2.26 (−2.05), −2.84 (−4.73), +4.69 (+7.41), −0.67 (−0.71), and −2.30 (−3.81) kJ mol^{-1}, which are corresponding to the electrostatic, exchange, repulsion, polarization and dispersion components, respectively, indicate that the electrostatic and dispersion interactions are the key attractive terms contributing significantly to the interaction energies of the OC···CH_3–F (CO···CH_3–F) complexes.

2.6   Natural bond orbital results

The reliability of the various geometrical, energetical, potential, and topological (QTAIM and NCI-RDG) signatures of the noncovalent interaction between CO and CH_3–X is further justified by natural bond orbital analysis. An application of this method is often emphasized in the literature to insight into the interorbital interactions between the monomers in the equilibrium complex geometries.[28-30] According to our calculations based on this theory, the O···C and C···C contacts are stabilized in part by charge

transfer delocalizations operating between the electron acceptor- and donor-NBOs, quantified by the second-order attractive energy term $E^{(2)}$ (see Eq. 1 of ESI). Among the other very small auxiliary contributions ($E^{(2)} \geq 0.21$ kJ mol^{-1}), the main charge transfer delocalization channels describing the O$\cdots$C interaction are in the direction: (1) from the oxygen lone-pair electron orbital n associated with the $V_{s,min}$ in CO to the σ^* anti-bonding orbtial of the C–X bond in CH$_3$–X (i.e., n(O) $\rightarrow$ σ^*(C–X)), and simultaneously, (2) that from both n of oxygen and π orbitals of the CO bond in CO to the 1-center Rydberg orbital RY* of the methylated carbon in CH$_3$–X (i.e., n(O) $\rightarrow$ RY*C and π(3)C$\equiv$O $\rightarrow$ RY*C, respectively). In the C$\cdots$C bonded interactions, the main charge transformer delocalization channel is centered between the carbon lone pair electron orbital n' in CO and the σ^* C–X anti-bond of CH$_3$–X, i.e., n'(C) $\rightarrow$ σ^*(C–X). The estimated energies $E^{(2)}$ for the above delocalizations amount to values between 0.3 to 1.3 kJ mol^{-1} for O$\cdots$C interactions, and that between 0.5 to 1.7 kJ mol^{-1} for C$\cdots$C interactions, obtained using NBO 3.0.[62]

2.7   Dipole moment and its changes

The molecular electric dipole moment, μ, is a measure of the degree of charge asymmetry in chemical compounds. Therefore, larger the dipole moment of the molecule larger is its polarity. The calculated (and experimental[63-64]) monomer dipole moments are ca. 3.76 (3.46), 4.06 (3.92), 2.01 (1.85), 2.07 (1.87), 2.02 (1.81), 1.86 (1.70), 2.50 (2.32), 1.97 (1.78) and 1.31(1.41) D for CH$_3$–NO$_2$, CH$_3$–CN, CH$_3$–F, CH$_3$–Cl, CH$_3$–Br, CH$_3$–OH, CH$_3$–CF$_3$, CH$_3$–Cl$_3$, and CH$_3$–NH$_2$, respectively, elucidating a reasonable agreement between theory and experiment. Similarly, the dipole moment of the CO molecule is computed to be 0.09 D which is in excellent agreement with the value 0.112 D observed experimentally.[63]

The D$\cdots$CH$_3$–X binary complexes are found to be all polar, each having its own permanent dipole moment. The smallest and the largest values of this are ca. 1.40 (1.41) and 4.13 (4.34) D for the O$\cdots$C (C$\cdots$C) bonded complexes involving CH$_3$–CN and CH$_3$–NH$_3$, respectively. And, relative to the sum of the monomer dipole moment values, $\Delta\mu$, the dipole moment of the complexes are seemingly either increased or decreased (see Table 1 for details). The decreasing tendency of $\Delta\mu$ is persistent with the O$\cdots$C bonded complexes, and an opposite attribute is discernible for most of the C$\cdots$C bonded complexes (except for OC$\cdots$CH$_3$–OH and OC$\cdots$CH$_3$–NH$_2$ for which $\Delta\mu < 0$, arising due to their bent intermolecular geometries). The unprecedented feature that isolates the O$\cdots$C from the C$\cdots$C bonded interactions is caused by the

electrostatic polarization of the CO molecule when its dipole moment directed towards, and away from, its interacting partner.

2.8 Atomic charges and their rearrangements

Illustrated in Figures 1 are also the integrated QTAIM charges q distributed on the atoms in the nine monomers. Do the space partitioning model derived charges give reasonable insights into the chemistry of unsubstituted and substituted compounds? Yes. Firstly, this is evident of the dipole moment data discussed in 2.7 above, in which, the assigned atomic charges faithfully reproduce the experimentally measured dipole moment values for the monomers. Secondly, let us look at the charges assigned to atoms in unsubstituted CH_4 (see Figure 1i). As can be readily seen, each H–atom in it is assigned with a positive average charge of +0.0144 e, while the carbon with a negative charge of −0.0577 e with PBE0/6–311++G(d,p). The negative charge of the carbon classically explains why each face of the tetrahedral carbon can serve as a representative of an H-bond acceptor, such as in $H_4C\cdots HY$ (Y = F, Cl, CN, OH), for example.[13,65] This specific quality of the molecule is also supported by the electrostatic surface potential model calculation, in which, there are four electrostatic potential minima on the surface of the carbon, each on the extension of an H–C bond (each with $V_{s,min}$ = −3.1 kcal mol^{-1}). By contrast, in the substituted systems H_3C–X (see from a to h of Figure 1), which are obtained by replacing an H-atom in CH_4 by an electron-withdrawing group –X, the $–CH_3$ carbon charge is positive. Concomitant with this there are positive areas of electrostatic potential on the surface of the carbon in H_3C–X on the extension of the C–X bond, explaining the reason why the methylated carbon in H_3C–X can act as a σ-hole donor.[12]

The distributions of the atomic charges in the $O\cdots C$ and $C\cdots C$ bonded complexes are shown in Figures 3 and 4, respectively. Clearly, one sees from these that there is a redistribution of the atom centered charges passing from the monomers to the complexes. The magnitude of the $–CH_3$ carbon charge in $CO\cdots CH_3$–X, as well as that in $OC\cdots CH_3$–X, relative to its value in isolated CH_3–X, increases, making it more electropositive. By contrast, the magnitudes of the carbon and oxygen charges in isolated CO on the formation of the $OC\cdots CH_3$–X complexes decrease, and that on the formation of the $CO\cdots CH_3$–X complexes increase (q(C) = −1.1658 e, q(O) = −1.1661 e for isolated CO). These most important changes are often considered as informative as they are directly associated with the intermolecular atomic pairs. [6,12,13,15,39,52-54]

As can be seen from Figures 3 and 4, the charges distributed on intermolecular pair of bonded atoms follow the patterns, $C^{\delta+}\cdots C^{\delta+}$ and $O^{\delta-}\cdots C^{\delta+}$, for the $OC\cdots CH_3–X$ and $CO\cdots CH_3–X$ complexes, respectively. Are these above patterns physically meaningful? Yes, they do. Firstly, '$-\cdots+$' obeys the classical law in which the two atoms in the intermolecular motif are having charges of opposite signs. Secondly, in the '$+\cdots+$' bonded pairs the magnitude of the charge on one atom is significantly larger than from that on the other, showing a depleted charge density profile in one and the concentration of that on other, a feature which may be necessary for the two atoms to be bonded. These types of charge arrangements are also previously described in dihydrogen-,[39,68] and H—H bonding interactions, [39, 66-68] in which cases, the signs of the charges on the acidic and hydridic H-atoms in the former were opposite to each other and that in the latter were identical. In analogy with this, together with the fact that the two bonded carbons in the C$\cdots$C pair are having opposite electrostatic surface potentials, one may therefore refer the interaction to as "dicarbon bonding", a new interaction yet to be exploited.

2.9   Vibrational characteristics

Another very important feature that is often used for decades to characterize the nature of an intermolecular interaction is the vibrational shift. This shift is commonly associated with the fundamental stretching frequencies of the covalent bonds linked directly with the electron-donor and -acceptor atoms of the two participating molecules. Table 3 summarizes the vibrational shifts $\Delta\omega$, the changes in the bond distances Δr, and the changes in the infrared intensities ΔI associated with the CO bond upon the formations of the $CO\cdots CH_3–X$ and $OC\cdots CH_3–X$ complexes (all the changes are given relative to the corresponding values in isolated CO). As can be seen from this table, there is a very distinguished pattern in $\Delta\omega$, classifying whilst the $CO\cdots CH_3–X$ complexes to exhibit a characteristic red-shift ($\Delta\omega < 0$), the $OC\cdots CH_3–X$ complexes to a characteristic blue-shift ($\Delta\omega > 0$) in $\omega(CO)$. Concomitant with the red- and blue-shifts are an increase and a decrease in the CO bond lengths for the former and latter complexes, respectively, in agreement with the IUPAC.[69,70] For both the cases, the infrared intensity of the CO band increases. We did not list the vibrational frequency shifts associated with the C–X bond of the $CH_3–X$ monomer in the complexes, as are impure vibrations affected by motions due to the neighboring atoms. We only note that the frequencies of the C–X bonds for the most stable complexes formed of CCl_3CH_3 and CH_3NO_2 with both the orientations of the CO molecule are blue-shifted (e.g., $\Delta\omega \sim 0.04 - 0.5$ cm^{-1}).

The complexes of CO with CH_3F, CH_3CN, CH_3Cl, CH_3OH, CH_3Br, CF_3CH_3, and NH_2CH_3 are all red-shifted ($\Delta\omega \sim 0.2 - 4.4$ cm^{-1}).

2.10 Bond electron delocalization properties

Finally, we comment on one of the most important properties, called the bond electron delocalization index δ,[43,71-74] associated with the O⋯C and C⋯C interactions. It is a two-electron property. It is independent of the QTAIM bond critical point framework. It resembles the bond order of a chemical bond in many instances. And it is related to the number of electrons exchanged between a given pair of two atomic basins in molecules.[71-72] Within the single determinant closed-shell approximations, $\delta(\Omega_A, \Omega_B)$ is calculated by integrating the exchange-correlation hole density,[71-72] Eq. 3, where the indices a and b in summations run over all the N/2 occupied molecular orbitals, and S_{ab} (A) and S_{ab} (B) are the molecular orbital overlap integrals over the atomic basins Ω_A and Ω_B, respectively.

$$\delta(\Omega_A, \Omega_B) = 4\sum_a \sum_b S_{ab}(A)S_{ab}(B) \dots\dots\dots\dots\dots\dots\dots\dots(3)$$

The calculated $\delta(\Omega_O, \Omega_C)$ and $\delta(\Omega_c, \Omega_C)$ values are depicted in Figures 3 and 4 for most of the O⋯C and C⋯C interactions, respectively. These values are considerably smaller, and are all below 0.02, regardless of nature of the interactions investigated. For instance, the $\delta(\Omega_O, \Omega_C)$ and $\delta(\Omega_c, \Omega_C)$ are ca. 0.0123 and 0.0171 for the noncovalent interactions in the CO⋯CH_3Br and OC⋯CH_3Br bonded complexes, respectively. And that these indices are in the range from 0.0088 and 0.0140 for O⋯C interactions, and are in the range from 0.0166 and 0.0200 for C⋯C interactions, in agreement with the order of stability found for these interactions (*vide supra*). By contrast, the covalently bonded atom pairs are associated with very large δ values (several orders of magnitude larger than the noncovalently bonded interactions) . For instance, the delocalization indices are approximately 0.68 for O–H, 0.88 for N–H, 0.92 for C–O, 0.93–0.96 for C–H, 0.91-1.07 for C–C, 1.03 for C–N, 0.84 for C–F, 1.09 for C–Cl, 1.13 for C–Br, 1.80 for C=O, and 2.40 for C≡N bonds. The significantly large δs are apparently due to the very short interatomic distances and the involvement of more number of exchanged electrons in the covalently bonded atom pairs.

Figures 8(a) and 8(b) illustrates the bcp charge density values are plotted against bond delocalization indices for the O⋯C and C⋯C interactions, respectively. Dependencies between local energy densities (kinetic, potential, and total) and bcp charge densities, and that between the intermolecular bond distances and the latter property, are displayed in Figures 8(c) and 8(d) for the O⋯C

bonded interactions, respectively. Figures 8(e) and 8(f) represent to the corresponding dependencies for C···C interactions, respectively. These sorts of relationships between one- and two-electron properties are previously established for covalent bonds,[43,74] metal-ligand bonds,[54] H-bonds, [75-76] dihydrogen bonds,[75] and H—H bonds. [44,77]

3. Summary

This paper presented the electronic structures and properties of eighteen weakly-bound intermolecular complexes of van der Waals type. We discussed nine of them, CO···CH$_3$–X, are formed between the outer end of the oxygen in CO and the methylated carbon end in the hydrophobic part of the CH$_3$–X molecules. The other nine, OC···CH$_3$–X, are formed by inverting the position of oxygen in the former nine complexes. The binding energies of the eighteen complexes are estimated to be too low, ranging between −1.01 and −2.30 kJ mol^{-1} for the CO···CH$_3$–X complexes, and that between −1.06 and −3.10 kJ mol^{-1} for the OC···CH$_3$–X complexes. The very small difference in the binding energies of the two interaction types for a given σ–hole donor is a consequence the counterbalance of the basicity and electronegativity on the carbon with that on the oxygen in the CO molecule.

The formations of the O···C and C···C interactions are concordant with an electrostatic surface potential description. For instance, we showed that there are two negative regions of electrostatic potential, each on each of the atomic surfaces of the CO molecule, on the outmost extension of the CO bond. These each individually prone to engage in bonding with the methylated carbon's positive area V$_{s,max}$ of electrostatic potential in CH$_3$–X.

The stable most complex (albeit very weak) of the eighteen series is roughly having a C$_s$ point group symmetry, with the CH$_3$–X is accompanied with the strongest electron deactivating substituent – NO$_2$. This was not unexpected as this group, compared to the other eight in the series, created the largest σ–hole on the surface of the carbon atom covalently bonded to it. We found no straightforward relationship between the carbon σ–holes in CH$_3$–X and the binding energies, as well as that between the former property and the internuclear distances of separation for the D···CH$_3$–X complexes.

The QTAIM and NCI-RDG charge density criteria are supportive of the formations of the O···C and C···C bonded pairs, and explained the interactions are of electrostatic origin. The NBO treatment described the O···C bond as the result of the charge transfer from the outer-end oxygen lone pair electron (and the π-electron) orbital of the CO molecule to the σ*(C–X) and RY*(C) anti-bond orbitals of

the CH_3–X molecules, whereas the C···C bond as a result of charge transfer from the outer-end carbon lone pair electron orbital of the CO bond to the $\sigma^*(C–X)$ orbital of the CH_3–X molecules.

We showed that whereas the recently proposed IUPAC criterion, the intermolecular bond distance is less than the sum of the van der waals radii of two bonded atoms, retains for most of the O···C bonds, this is so not for most of the C···C bonds, as in this latter case the predicted C···C bond distances are too large (3.52 – 3.81 Å).

A vibrational normal mode analysis suggested that the CO stretching frequencies of the O···C bonded interactions are to be red-shifted, whereas that of the C···C interactions are to be blue-shifted. These vibrational shifts are shown to be associated with an increase and a decrease in the CO bond distances for the corresponding complexes, respectively. And in all the cases, the infrared intensity is found to be increased. The C–X bonds in the complexes, on the other hand, displayed characteristic red-shifts in their corresponding stretching frequencies for the OC···CH_3–X bonded complexes, except for the four most stable complexes formed of CO upon its interaction with CH_3–NO_2 and CH_3–Cl_3, which are all blue-shifted.

The integrated QTAIM charges are analyzed to show that the sign and magnitude of atomic charges alone are insufficient to tell the details of positive and negative sites on atoms in molecules. However, they can be used to infer whether the atom of interest can at least be a representative of an electrophillic or a nucleophillic attack in molecules. We have showed that there were charge redistributions accompanying formation of the OC···CH_3–X and CO···CH_3–X complexes. Also, we showed that the patterns, $C^{\delta+}$···$C^{\delta+}$ and $O^{\delta-}$···$C^{\delta+}$, are persistent with majority of the OC···CH_3–X and CO···CH_3–X complexes investigated, respectively. Based on a previous report,[12] we characterized the O···C interaction to 'carbon bond'. And, in analogy with dihydrogen bonding, we suggest the C···C interactions to be referred to as 'dicarbon bonds', yet another specific to be exploited in detail.

As already discussed in the Introduction, the ubiquitous carbon bonded interactions are not only crucial for the fundamental understanding of the S_N2 reactions, but also it is expected that they find application in anion binding and host-guest supramolecular chemistry. For instance, our on-going research on the occurrence of the present phenomena concerns with the other contexts, wherein the combination of several methane derivatives and a cyanide anion allowed us identifying several anion receptor hosts for carbon- and dicarbon-bonds, and we present our work elsewhere.

References

1. A. C. Legon, Phys. Chem. Chem. Phys. 2010, 12, 7736.

2. F. Meyer, P. Dubois, Cryst. Eng. Comm. 2013,15, 3058.

3. L. Pauling, The nature of the chemical bond and the structure of molecules and crystals: An introduction to modern structural chemistry, 2nd Edition. Cornell University Press, Ithaca, N. Y., 1940.

4. J. Klimes, A. Michaelides, J. Chem. Phys. 2012, 137, 120901. References therein.

5. S. Scheiner, J. Chem. Phys. 2011, 134, 094315–094319.

6. P. R. Varadwaj, A. Varadwaj, G. H. Peslherbe, J. Comput. Chem. 2012, 33, 2073-82.

7. P. L. A. Popelier, J. Phys. Chem A 1998, 102, 1873.

8. J. S. Murray, P. Politzer, WIREs Comput. Mol. Sci.: Overview 2011, 1, 153 - 163.

9. U. Adhikari, S. Scheiner, Chem. Phys. Lett. 2012, 532, 31.

10. S. Scheiner, Int. J. Quantum Chem. 2013, 113, 1609.

11. Halogen Bonding, Fundamentals and Applications, ed. P. Metrangolo, G. Resnati, Springer-Verlag, Berlin, 2008.

12. D. Mani, E. Arunan, Phys. Chem. Chem. Phys. 2013, 15, 14377. References therein.

13. A. Bauzá, T. J. Mooibroek, A. Frontera, Angew. Che, Int. Ed. 2013, 18, 12317.

14. A. Bundhun, P. Ramasami, J. S. Murray, P. Politzer, J. Mol. Model. 2013, 19, 2739.

15. E. Arunan, Curr. Sci. 2013, 105, 892.

16. S. J. Grabowski, Phys. Chem. Chem. Phys. 2014, 16, 1824. References therein.

17. A. Bauzá, R. Ramis, A. Frontera, Comput. Theor. Chem. 2014, 1038, 19.

18. Qingzhong Li, Xin Guo, Xin Yang, Wenzuo Li, Jianbo Cheng and Hai-Bei Li, Phys. Chem. Chem. Phys. 2014, 16, 11617.

19. S. A. C. McDowell, Chem. Phys. Lett. 2014, 598, 1.

20. S. A. C. McDowell, J. A. Joseph, Phys. Chem. Chem. Phys. 2014, 16, 10854.

21. P. R. Varadwaj, A. Varadwaj, B.-Y. Jin (ms submitted).

22. L. M. Azofra, M. M. Quesada-Moreno, I. Alkorta, J. R. Avilés-Moreno, J. J. López-González, J. Elguero, New J. Chem., 2014, 38, 529.

23. S. P. Thomas, M. S. Pavan, T. N. G. Row, Chem. Commun. 2014, 50, 49.

24. (a) P. Hohenberg, W. Kohn, Phys. Rev. 1964, 136, B864; W. Kohn, L. J. Sham, Phys. Rev. 1965, 140, A1133; (b) W. Kohn, L. J. Sham, Phys. Rev. 1965, 140, A1133.

25. C. Adamo, V. Barone, J. Chem. Phys. 1999, 110, 6158.

26. R. F. W. Bader, Atoms in Molecules - A Quantum Theory, Oxford University Press, Oxford, 1990.

27. C. F. Matta, R. J. Boyd (Eds.), "The Quantum Theory of Atoms in Molecules: From Solid State to DNA and Drug Design", Wiley-VCH, Weinheim, 2010.

28. F. Weinhold, C. Landis, Valency and Bonding, A Natural Bond Orbital Donor-Acceptor Perspective, Cambridge University Press, New York, 2005.

29. I. V. Alabugin, M. Manoharan, S. Peabody, F. Weinhold, J. Am. Chem. Soc. 2003, 125, 5973-5987.

30. F. Weinhold, J. Comput. Chem. 2012, 33, 2363.

31. E R. Johnson, S. Keinan, P. Mori-Sanchez, J. Contreras-Garcia, A J. Cohen, and W. Yang, J. Am. Chem. Soc. 2010, 132, 6498.

32. J. Contreras-Garcia, E. Johnson, S. Keinan, R. Chaudret, J-P Piquemal, D. Beratan, W. Yang, J. Chem. Theor. Comp. 2011, 7, 625.

33. J. S. Murray, P. Politzer, Cryst. Eng. Comm. 2013, 15, 3145.

34. R. F. W. Bader, C. F. Matta, J. Phys. Chem. A 2004, 108, 8385.

35. A. Varadwaj, P. R. Varadwaj, Chem. Euro. J. 2012, 18, 15345.

36. B. Bankiewicz, P. Matczak, M. Palusiak, J. Phys. Chem. A 2012, 116, 452.

37. I. V. Alabugin, K. M. Gilmore, P. W. Peterson, WIREs Comput. Mol. Sci. 2011, 1, 109.

38. C. F. Guerra, F. M.s Bickelhaup, J. Chem. Phys. 2003, J119, 4262.

39. J. Hernández-Trujillo, C. F. Matta, Struct. Chem. 2007, 18, 849.

40. J. R. Lane, J. Contreras-García, J. P. Piquemal, B. J. Miller, Henrik G. Kjaergaard, J. Chem. Theory Comput. 2013, 9, 3263.

41. E. Espinosa, M. Souhassou, H. Lachekar, C. Lecomte, Acta Crystallogr. B 1999, 55, 563.

42. E. Espinosa, I. Alkorta, J. Elguero, E. Molins, J. Chem. Phys. 2002, 117, 5529.

43. C. F. Matta, J. Hernández-Trujillo, J. Phys. Chem. A 2003, 107, 7496.

44. I. Cukrowski, C.F. Matta, Chem. Phys. Lett. 499, 2010, 66.

45. T. A. Keith, AIMAll (Demo Version 11.03.14), 2011. Available via DIALOG at: http://im.tkgristmill.com.

46. Gaussian 09. For citation detail, see ref. 6 of supporting information.

47. T. Lu, F. Chen, J. Mol. Graph. Model. 2012, 38, 314.

48. S. Alvarez, Dalton Trans. 2013, 42, 8617.

49. R. F. W. Bader, J. Phys. Chem. A, 2009, 113, 10391.

50. A. M. Pendás, E. Francisco, M. A. Blanco, C. Gatti, Chem. Eur. J. 2007, 13, 9362.

51. R. F. W. Bader, Atoms in Molecules, in: Theoretical and Computational Chemistry, Encyclopedia of Computational Chemistry, Vol. 4, John Wiley & Sons, Ltd., 1998. This is available via DIALOGUE: http://www.wiley.com/legacy/wileychi/ecc/samples/sample02.pdf.

52. M. V. Vener, A. V. Manaev, A. N. Egorova, V. G. Tsirelson, J. Phys. Chem. A 2007, 111, 1155.

53. C. S. López, O. N. Faza, F. P. Cosso, D. M. York, A. R. de Lera, Chem. Eur. J. 2005, 11, 1734.

54. P. R. Varadwaj, H. M. Marques, Phys. Chem. Chem. Phys. 2010, 12, 2126.

55. T. T. T. Bui, S. Dahaoui, C. Lecomte, G.R. Desiraju, E. Espinosa, Angew. Chem. Int. Ed. 2009, 48, 3838.

56. W. Nakanishi, S. Hayashi, K. Narahara, J. Phys. Chem. A 2008, 112, 13593.

57. R. A. Cormanich, M. A. Moreira, M. P. Freitas, T. C. Ramalho, C. P. A. Anconi, R. Rittner, R. H. Contreras, C. F. Tormena, Magn. Reson. Chem. 2011, 49, 763–767.

58. J. A. Pople, M. Heas-Gordon, K. Raghavachari, J. Chem. Phys. 1987, 87, 5968.

59. X. Lu, H. Li, X. Zhu, W. Zhu, H. Liu, J. Phys. Chem. A, 2011, 115, 4467.

60. A. J. A. Aquino, D. Tunega, G. Haberhauer, M. H. Gerzabek, H. Lischka, J. Phys. Chem. A, 2002, 106, 1862.

61. S. F. Boys, F. Bernardi, Mol. Phys. 1970, 19, 553.

62. NBO Version 3.1, E. D. Glendening, A. E. Reed, J. E. Carpenter, and F. Weinhold. Original literature, J. P. Foster and F. Weinhold, "Natural hybrid orbitals," J. Am. Chem. Soc. 1980, 102, 7211.

63. The experimental data of molecular structural, dipole moment, vibrational, and thermodynamic properties of all the monomers investigated in this study can be found in the NIST Computational Chemistry Comparison and Benchmark Database, NIST Standard Reference Database Number

101. Release 16a, August 2013, Editor: R. D. Johnson III. Available via DIALOGUE: http://cccbdb.nist.gov/

64. R. D. Nelson Jr., D. R. Lide, A. A. Maryott "Selected Values of electric dipole moments for molecules in the gas phase" NSRDS-NBS10, 1967.

65. B. Raghavendra, E. Arunan, Chem. Phys. Lett., 2008, 467, 37. References therein.

66. H. Zaher, A. E. Ashley, M. Irwin, A. L. Thompson, M. J. Gutmann, T. Krämera, D. O'Hare, Chem. Commun. 2013, 49, 9755.

67. C. F. Matta, J. Hernández-Trujillo, T. H. Tang, R. F. W. Bader, Chem. Eur. J. 2003, 9, 1940.

68. Matta CF (2006) Hydrogen–hydrogen bonding: the non-electrostatic limit of closed-shell interaction between two hydrogen atoms. A critical review. In: Grabowski S (ed) Hydrogen Bonding—New Insight, (Challenges and advances in computational chemistry and physics series), Springer, pp 337–376.

69. G. R. Desiraju, Angew. Chem. Int. Ed. 50, 2011, 52.

70. G. R. Desiraju, P. Shing Ho, L. Kloo, A. C. Legon, R. Marquardt, P. Metrangolo, P. Politzer, G. Resnati, K. Rissanen, Pure Appl. Chem. 2013, 85, 1711.

71. R. F. W., Bader, M. E. Stephens, J. Am. Chem. Soc. 1975, 97, 7391.

72. X. Fradera, M. A. Austen, R. F. W. Bader, J. Phys. Chem. A 1999, 103, 304.

73. E. Matito, J. Poater, M. Solá, M. Duran, P. Salvador J. Phys. Chem. A 2005, 109, 9904.

74. C. L. Firme, O. A. C. Antunes, P. M. Esteves, Chem. Phys. Lett. 468, 2009, 129.

75. S. J. Grabowski, Croat. Chem. Acta 2009, 82, 185.

76. D. Hugas, L. Guillaumes, M. Duran, S. Simon, Comput. Theor. Chem. 2012, 998, 113.

77. P. R. Varadwaj, A. Varadwaj, G. H. Peslherbe, H. M. Marques, J. Phys. Chem. A, 2011, 115, 13180.

78. P. Su, H. Li, J. Chem. Phys. 2009, 131, 014102.

79. M. W. Schmidt, K. K. Baldridge, J. A. Boatz, S. T. Elbert, M. S. Gordon, J. H. Jensen, S. Koseki, N. Matsunaga, K. A. Nguyen, S. J. Su, T. L Windus, M. Dupuis, J. A. Montgomery, J. Comput. Chem. 1993, 1, 1347.

80. P. Piecuch, S. A. Kucharski, K. Kowalski, M. Musial, Comp. Phys. Commun. 2002, 149, 71.

TOC

Illustrated is an example of a 'dicarbon bond' formed between a pair of two carbon atoms of the $OC\cdots CH_3$-Cl_3 intermolecular complex, one corresponding to the methylated carbon in 1,1,1-trichloro-ethane (CH_3-Cl_3) and one to the carbon in the carbon dioxide (CO) molecule, where the three dots '$\cdots$' represent to the noncovalent interaction, and the lines in atom color represent to the interatomic basin paths for selected atoms of the complex.
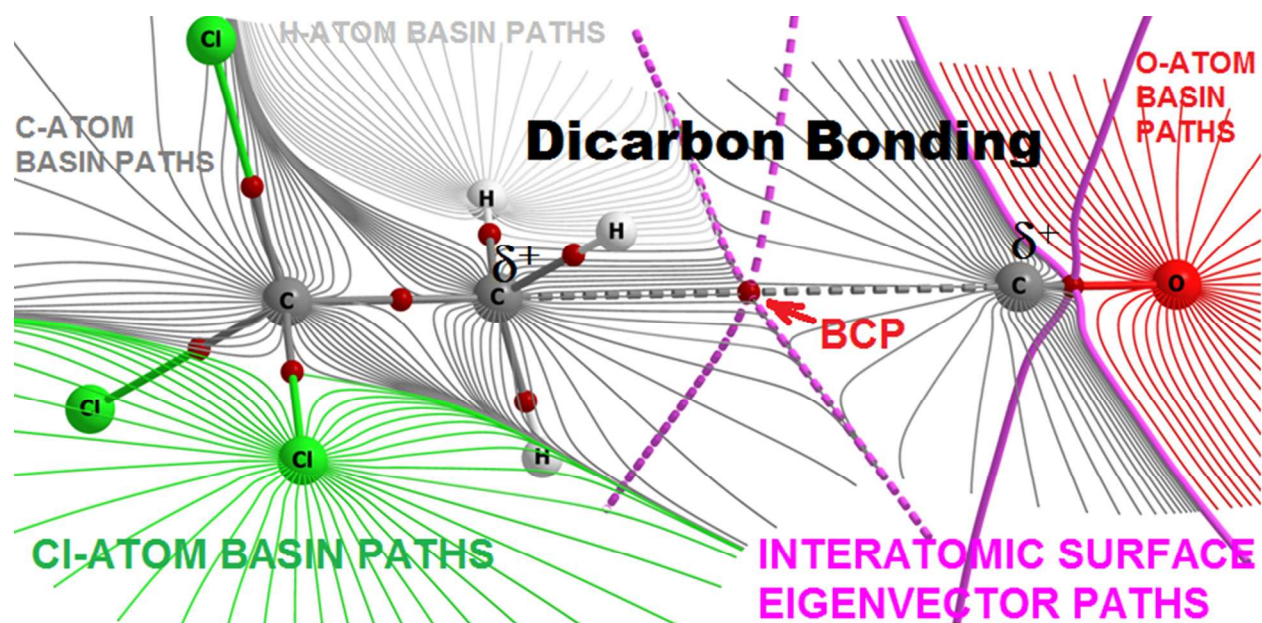
Figure 1: QTAIM molecular graphs for some selected monomers investigated, obtained using the PBE0/6–311++G(d,p) level of theory. These include CH_3-NO_2 (a), CH_3-CN (b), CH_3-F (c), CH_3-Cl (d), CH_3-NH_2 (e), CH_3-OH (f), CH_3-CF_3 (g), CH_3-Cl_3 (h), and CH_4 (i). The integrated QTAIM atom charges (numbers in blue) and bond critical point charge densities (numbers in black) are given for all cases. The bond paths representing to the covalent interactions in atom pairs are illustrated as solid lines in atom color (F in lime, Cl in deep-lime, C in gray, O in red, and H in white-gray). The bond critical points in bonded atomic pairs lying along the bond paths are shown as tiny spheres in darkred.
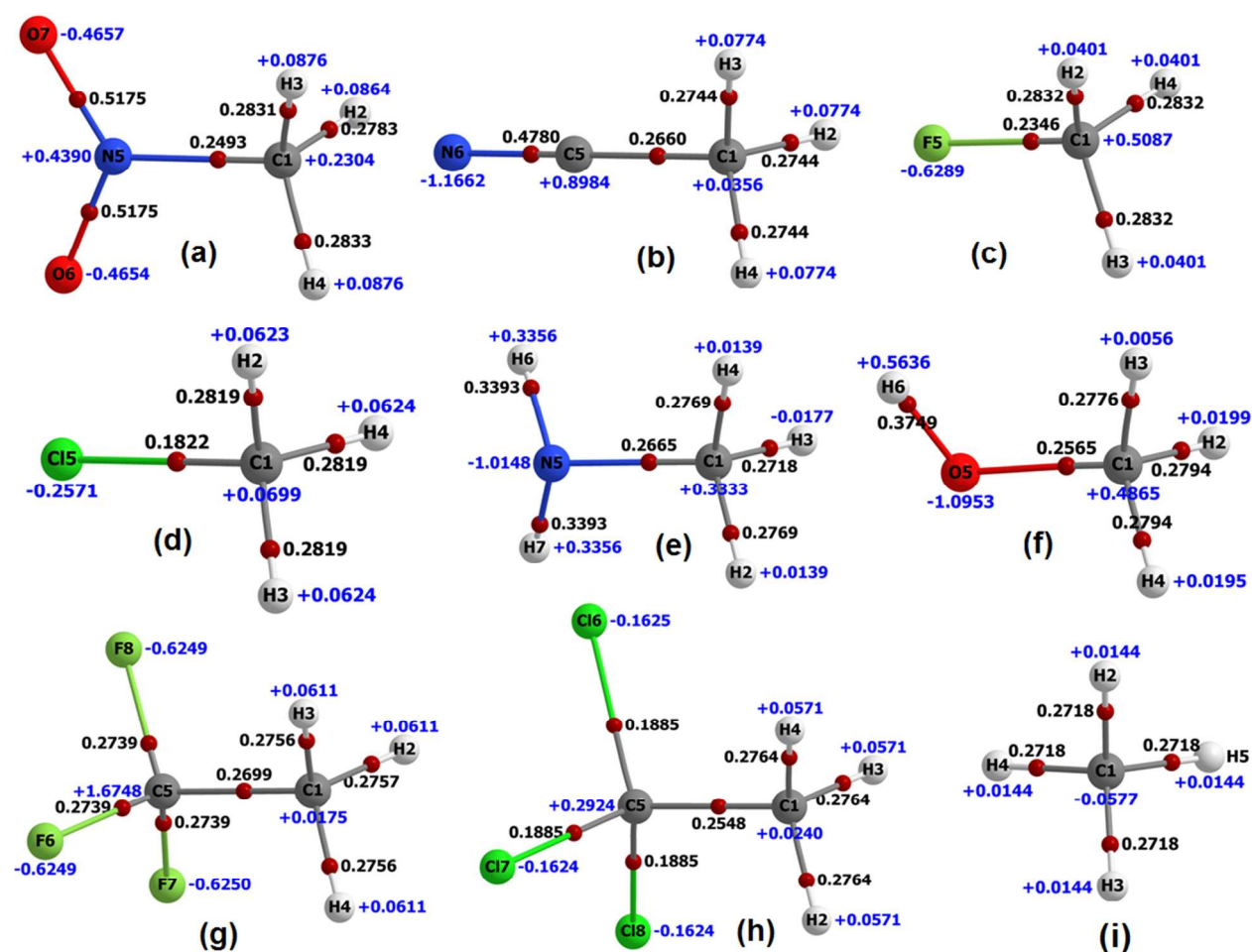
Figure 2: PBE0/6–311++G(d,p) electrostatic surface potentials mapped on the corresponding 0.001 au electron density isosurfaces of (a) CH_3–CCl_3, (a') CCl_3–CH_3, (b) CH_3–F, and (c) CO. The –CCl_3, –CH_3 and –F fragments in the former three species are in the background, while the positions of the carbon and oxygen in isolated CO are similar to those in its molecular graph (ball and stick model in (c)). Unless otherwise mentioned, the electrostatic surface potential values are in kcal mol^{-1}, the bond path between the two atoms in CO is in atom color, and the bcp along the bond path as a small sphere in dark-red. The regions with the most negative and most positive electrostatic surface potentials, $V_{s,min}$ and $V_{s,max}$, are color coded with red and blue, respectively.
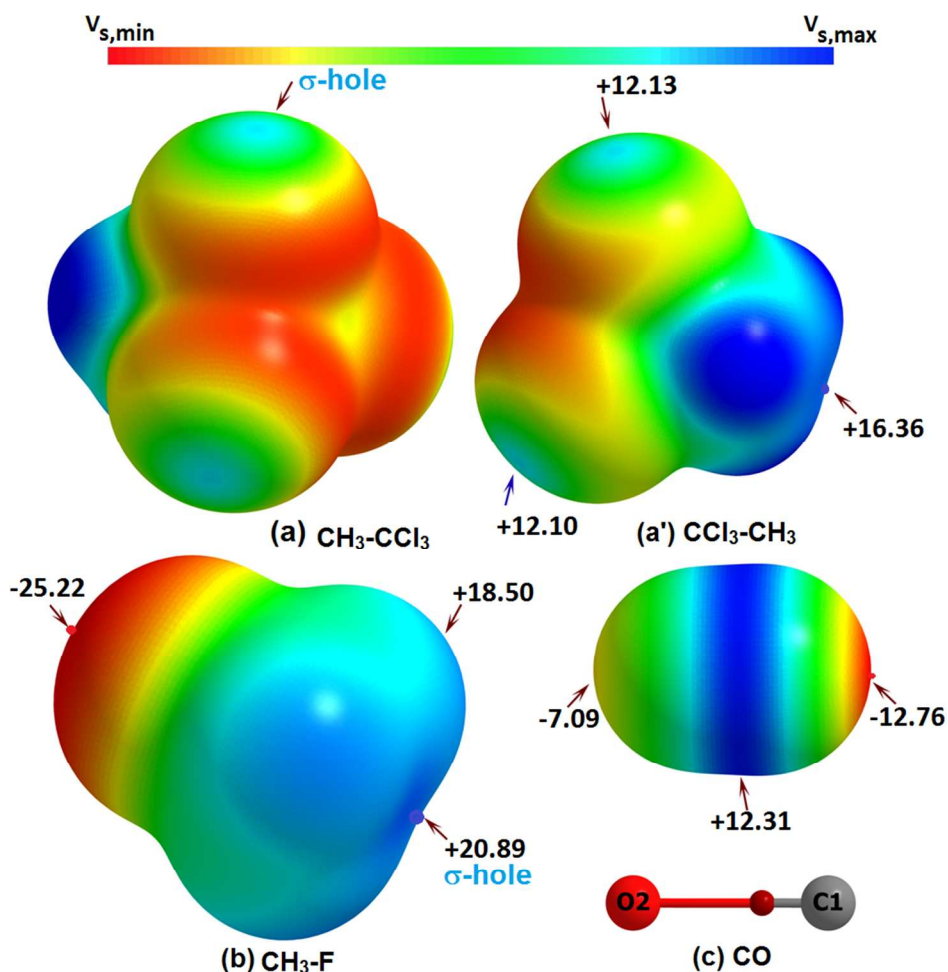
Figure 3: QTAIM molecular graphs for most of the O···C bonded binary complexes, computed with PBE0/6-311++G(d,p). The bond paths representing to the covalent (solid lines) and weak (dotted lines) interactions between atomic pairs in the complexes are illustrated in atom color (F in lime, Cl in deep-lime, C in gray, O in red, and H in white-gray). The bond critical point in each bonded atomic pair lying along the bond path is shown as a tiny sphere in dark-red. The integrated QTAIM atom charges (values in blue), and the second eigenvalue of the Hessian of charge density (λ_2) values at bcps (values in black), are given for all shared interactions, while the delocalization indices $\delta(\Omega_O,\Omega_C)$ (values in green) are listed only for the closed-shell interactions. Units of charge and λ_2 are in e and au, respectively (1 au of λ_2 = 24.099 eÅ^{-5}). Atom labeling is randomly shown.
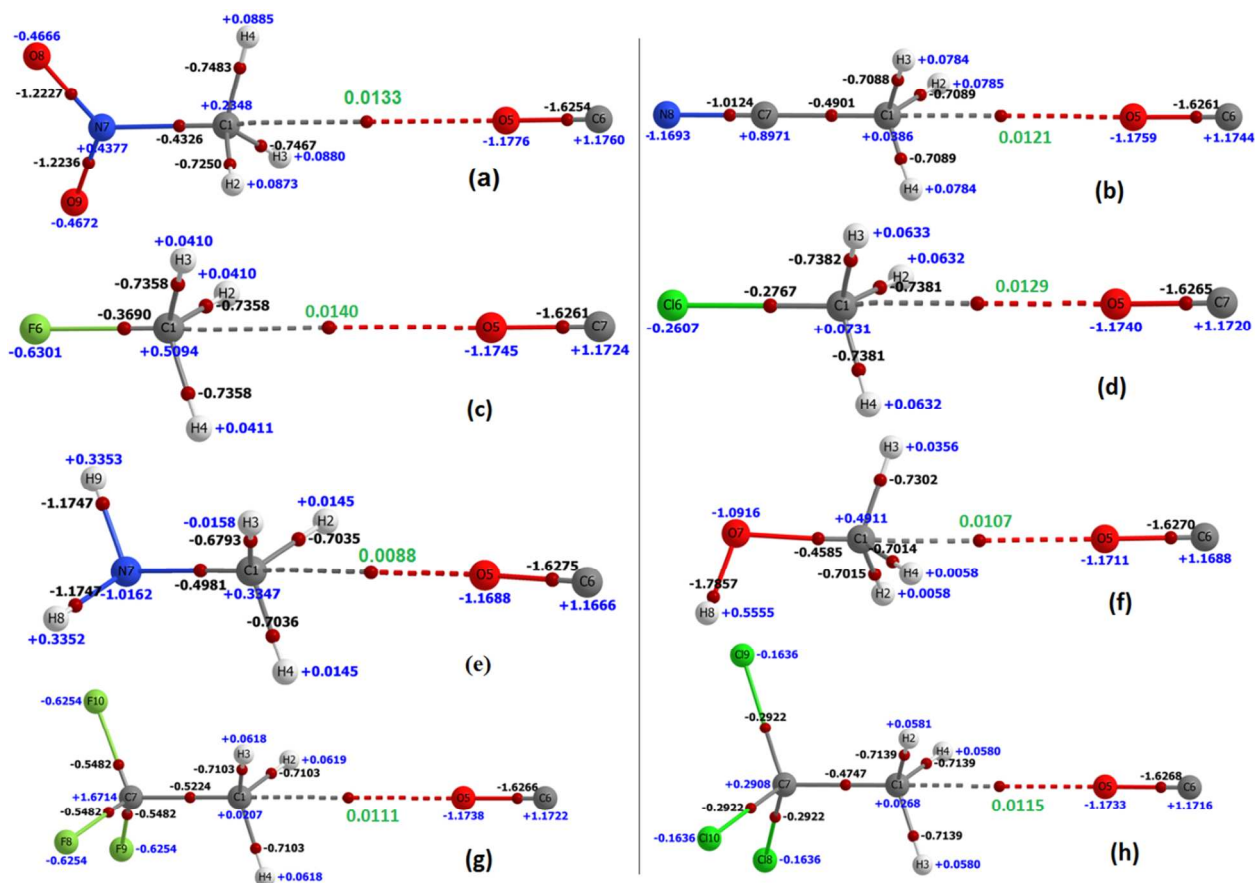
Figure 4: QTAIM molecular graphs for most of the C···C bonded complexes, computed with PBE0/6-311++G(d,p). The bond paths representing to the covalent (solid lines) and weak (dotted lines) interactions between atomic pairs in the complexes are illustrated in atom color (F in lime, Cl in deep-lime, C in gray, O in red, and H in white-gray). The bond critical point in each bonded atomic pair lying along the bond path is shown as a tiny sphere in dark-red. The integrated QTAIM atom charges (values in blue), and the second eigenvalue of the Hessian of charge density (λ_2) values at bcps (values in black), are given for all shared interactions, while the delocalization indices $\delta(\Omega_C,\Omega_C)$ (values in green) are listed only for the closed-shell interactions. Units of charge and λ_2 are in e and au, respectively (1 au of $\lambda_2 =$ 24.099 eÅ^{-5}). Unless otherwise indicated, each structure is a minimum, except (g), which is a second order saddle point. Atom labeling is randomly shown.
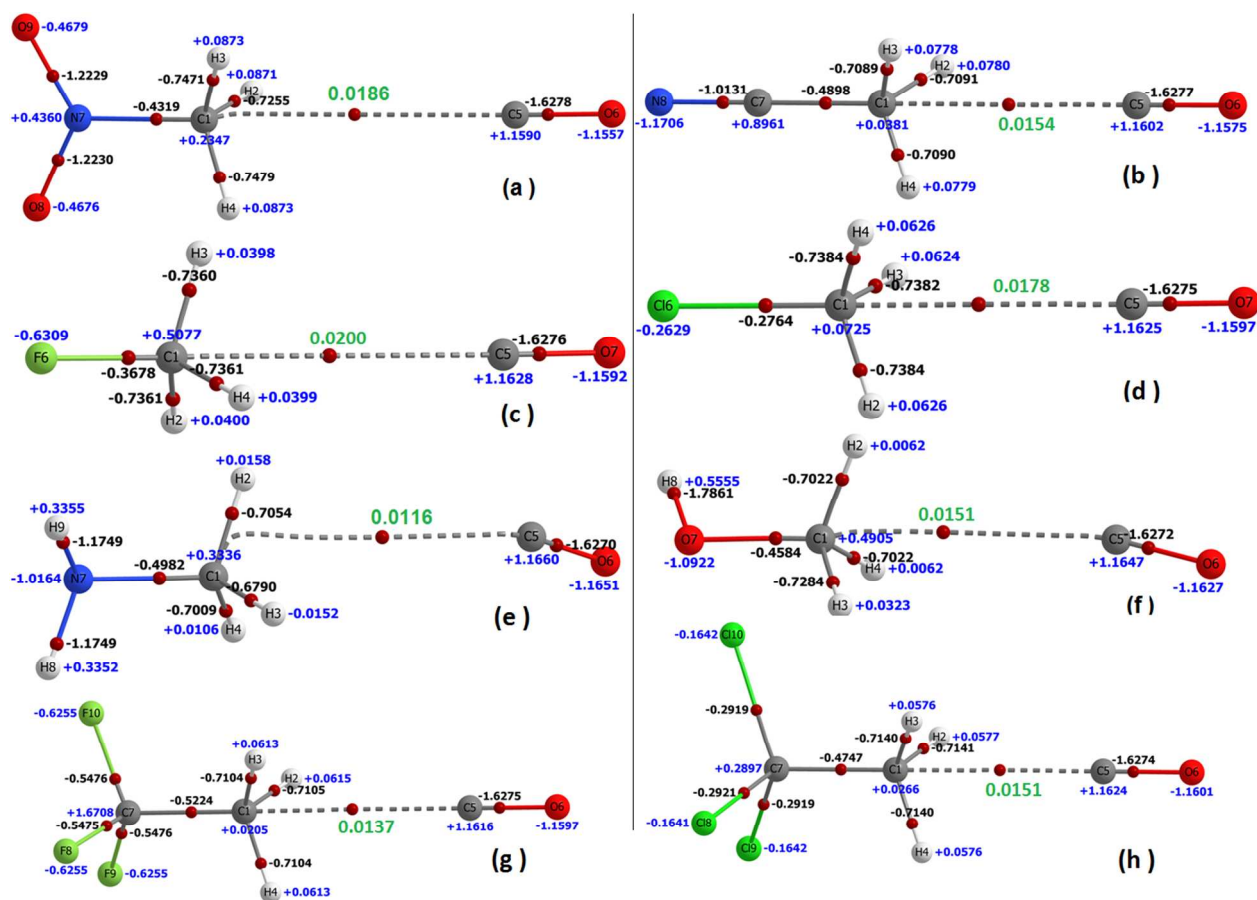
Figure 5: Examples showing contour plots of the Laplacian of the charge density for CH_3-Br (a), CH_3–CCl_3 (b), OC···CH_3–Br (c), and CO···CH_3–CCl_3 (d). Regions of charge-concentration (dotted lines in red, $\nabla^2\rho_b < 0$) and -depletion (solid lines in blue, $\nabla^2\rho_b > 0$) are marked with blue- and red-arrows, respectively. The bond path between each atom pair of two nuclei painted in solid and dashed lines in atom-color represent to the shared- and closed-shell interactions, respectively, while the tiny spheres painted in dark-red represent to the bond critical points. The charge depleted regions lying along the outer extensions of the Br–C and C–C bond axes, as in (a)-(d), reveal the presence of σ-holes. Atom labeling is randomly illustrated.

σ−hole
(regions of charge depletion)

Regions of charge depletion

$\nabla^2\rho > 0$

Regions of charge concentration $\nabla^2\rho < 0$

(a) CH₃Br

(b) CH₃-CCl₃

(c) OC···CH₃Br
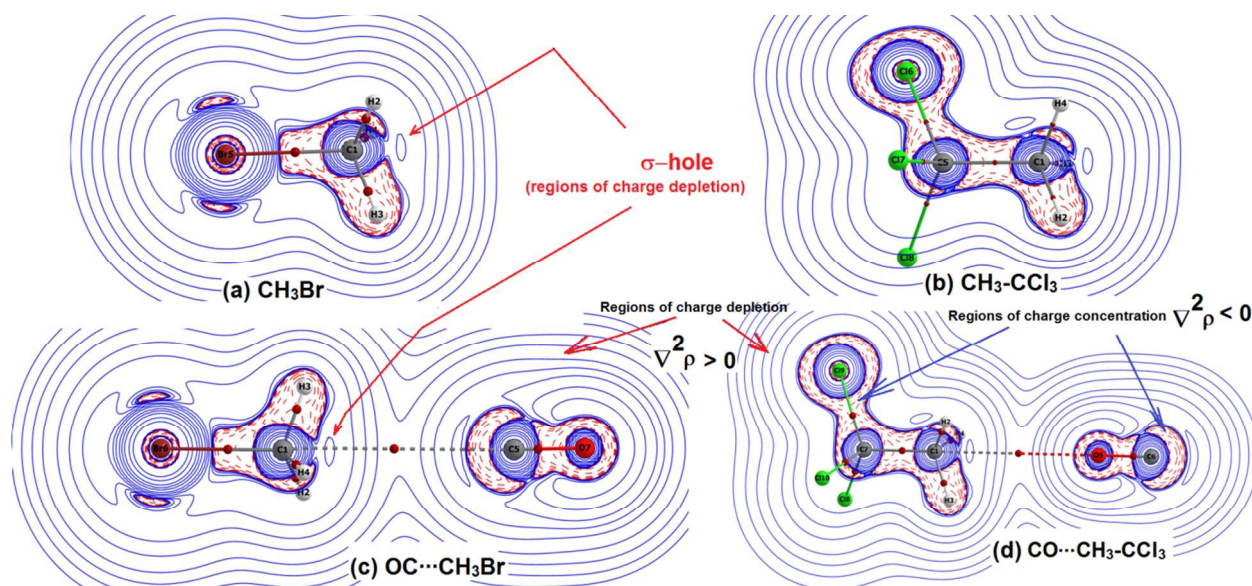
(d) CO···CH₃-CCl₃

Figure 6: An example showing the relief maps of the Laplacian of the charge density for the CO$\cdots$CH$_3$–CCl$_3$ (a) and OC$\cdots$CH$_3$–CCl$_3$ (b) bonded complexes truncated at an height of 7 au (1 au of $\nabla^2\rho_b$= 1e a$_0^{-5}$ = 24.099 eÅ^{-5}), with the former and the latter are in the plane defined by HCO and HCC, respectively. Color codes refer to red and yellow are the most and least negative values of $\nabla^2\rho_b$, respectively, while that to green, cyan, and blue are from the less positive to the most positive values of $\nabla^2\rho_b$ ($\nabla^2\rho_b$ varies from −1.0 (red) to +1.0 au (blue), where 1 au of $\nabla^2\rho_b$ = 24.099 eÅ^{-5}).
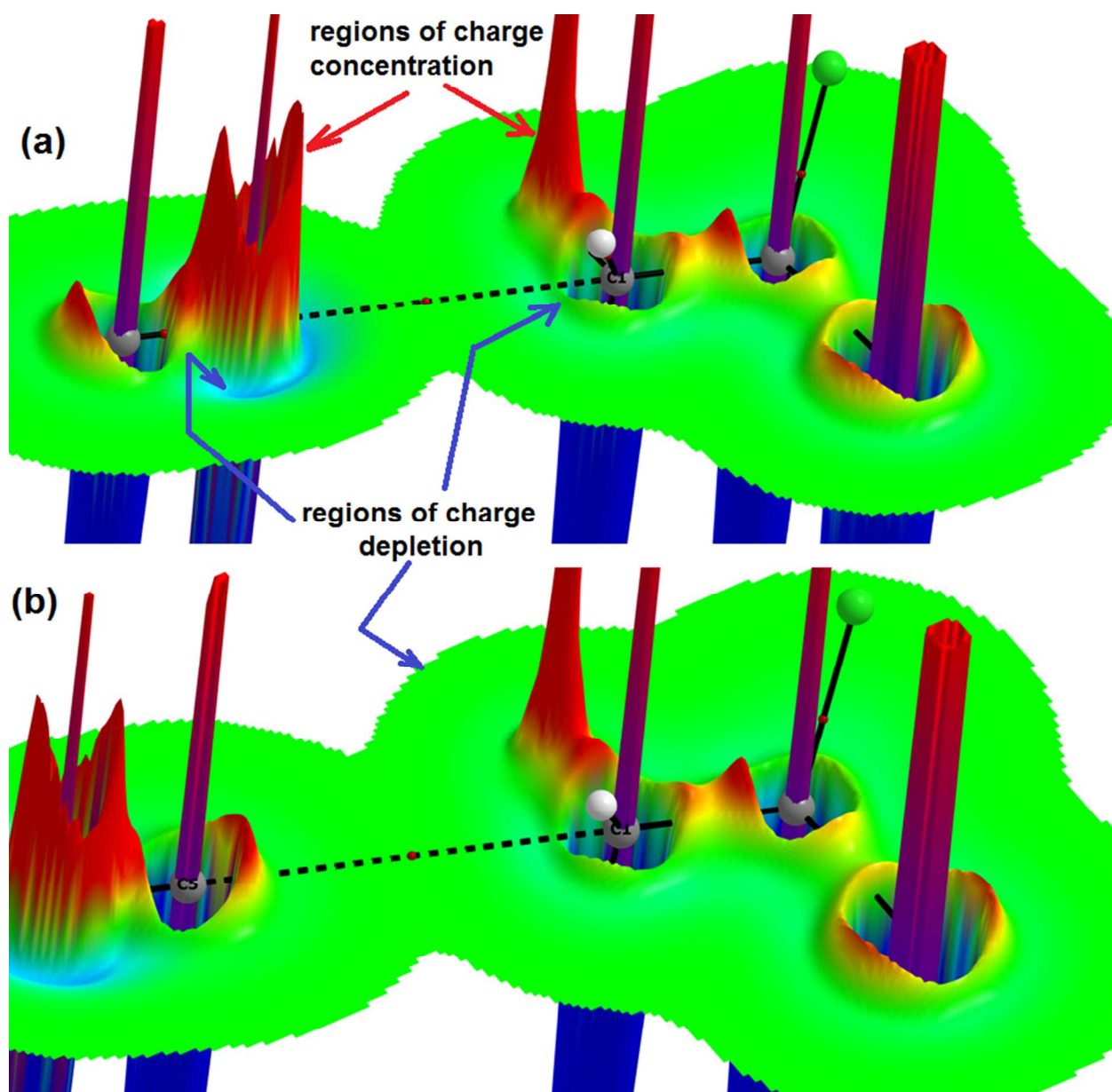
Figure 7: The NCI RDG s vs. sign(λ_2)ρ plots for some selected molecular complexes formed of either of the two orientations of the CO molecule and the σ–hole in CH$_3$–Cl$_3$ (a), CH$_3$–Br (b), and in CH$_3$–NH$_2$ (c). The troughs (spikes) on the left side of sign(λ_2)$\rho \cong 0$ represent to the weak interaction between the monomers in the complexes, and that of the small ones on right marked within blue circles by arrows are probably due to very weak secondary interactions caused by the hydrogens of the –CH$_3$ group in CH$_3$–X. The s = 0.5 au isosurfaces in the ball and stick models of the complexes representing to the weak interactions are shown by triangle-shaped green volumes in the intermolecular regions. Atom labeling is not depicted.
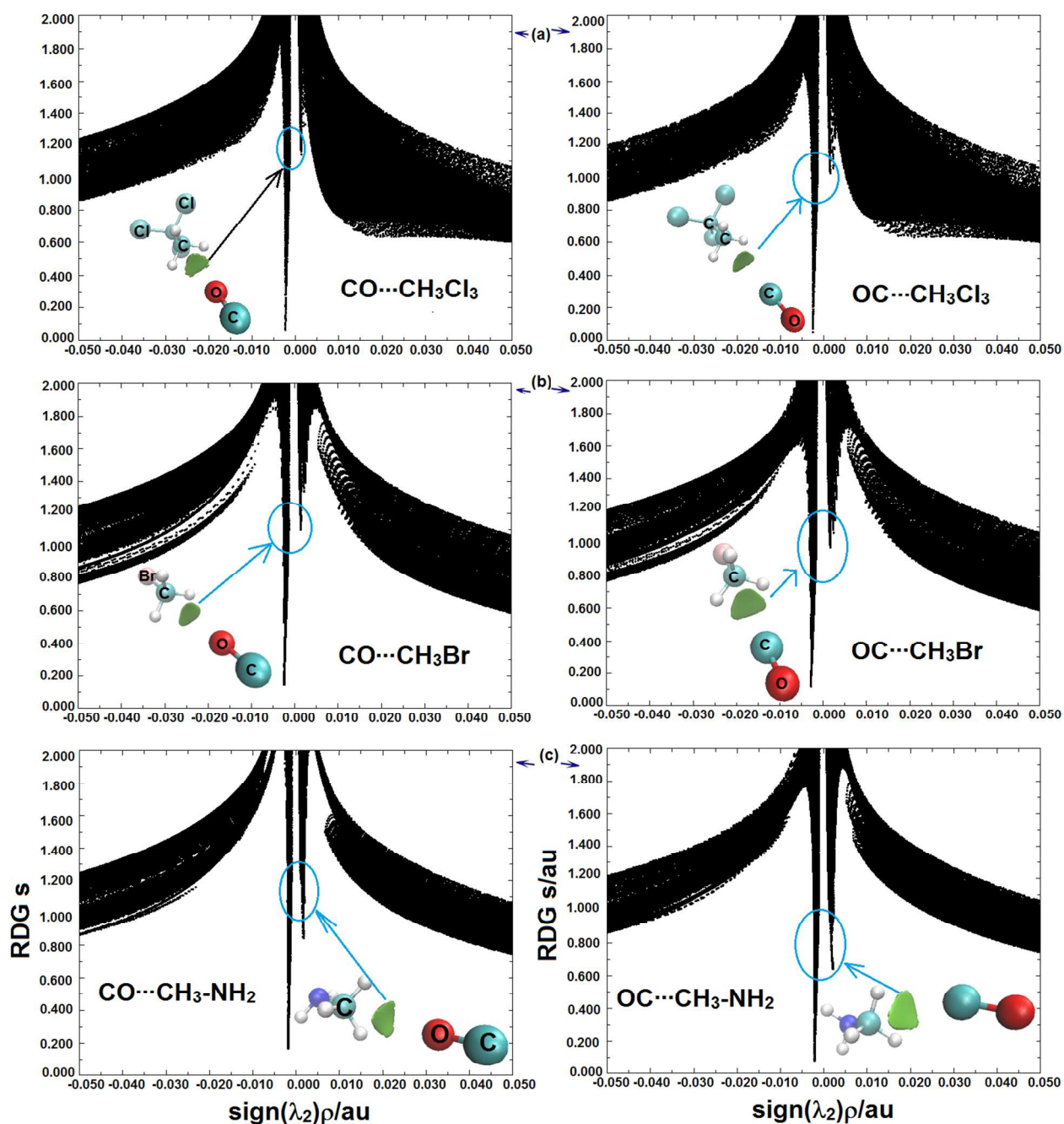
Figure 8: Dependence of the bcp charge density ρ_b on the bond delocalization index δ (a), on the energy densities (kinetic (G_b), potential (V_b), and total (H_b)) (b), and on the C$\cdots$O intermolecular bond distances for the C$\cdots$O bonded complexes, respectively. The corresponding relationships for the C$\cdots$C bonded complexes are shown in (b), (d), and (e), respectively, The red sphere in (b) is an outlier. For each case, the data are fitted to an exponential function. For the graphs in (e) and (f), the data are also fitted to a linear a function. The adjusted-square regression coefficient, R^2, is shown for each case.
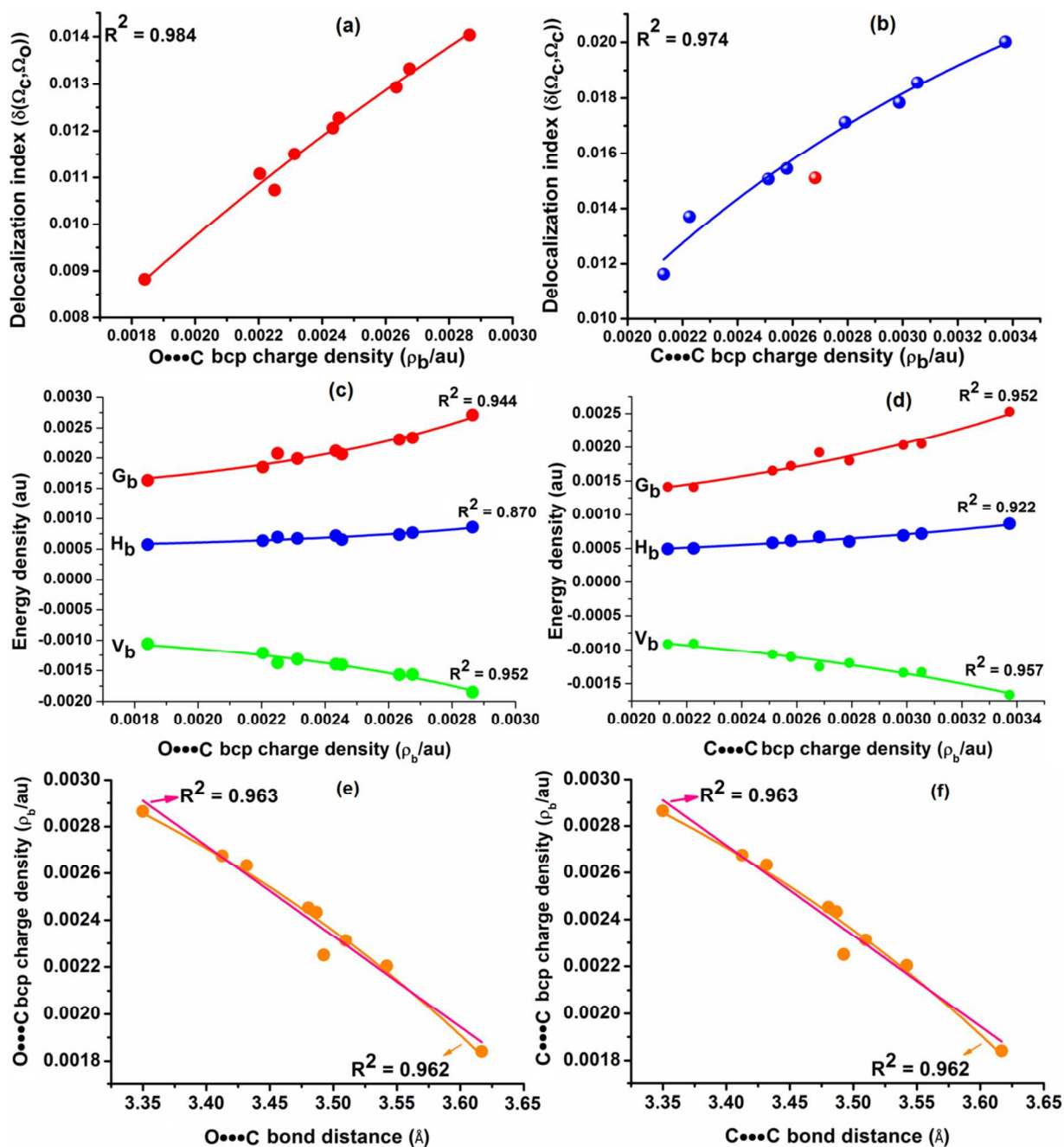
Table 1: Selected physical properties of the O···C and C···C bonded complexes, obtained via PBE0/6-311++G(d,p). The properties include the binding energies (ΔE/kJ mol^{-1}), the changes in the dipole moment values ($\Delta\mu$/D), the zero-point vibration corrected binding energies (ΔE^{zpe}/kJ mol^{-1}), the changes in the enthalpy values (ΔH/kJ mol^{-1}), the intermolecular distances (r/Å), and the carbon bond bond-angles ($\angle$/$^{\circ}$).

Complex	ΔE^a	$\Delta\mu^b$	ΔE^{zpe}	ΔH^c	r(C···O)	$\angle$C=O···C	Complex	ΔE^a	$\Delta\mu^b$	ΔE^{zpe}	ΔH^c	r(C···C)	$\angle$O=C···C
CO···CH$_3$NO$_2$	-2.30	-0.002	-1.64	1.39	3.412	179.42	OC···CH$_3$NO$_2$	-3.10	0.20	-2.24	0.67	3.608	178.40
CO···CH$_3$CN	-2.04	-0.03	-1.11	1.66	3.487	179.44	OC···CH$_3$CN	-2.53	0.18	-1.82	1.20	3.722	179.34
CO···CH$_3$F	-1.94	-0.07	-1.10	1.76	3.350	179.33	OC···CH$_3$F	-2.66	0.13	-1.47	1.08	3.516	179.36
CO···CH$_3$Cl	-1.89	-0.06	-0.98	1.82	3.432	179.26	OC···CH$_3$Cl	-2.33	0.15	-1.54	1.40	3.625	179.43
CO···CH$_3$Br	-1.64	-0.06	-0.97	2.07	3.480	179.15	OC···CH$_3$Br	-2.06	0.16	-1.44	1.67	3.677	178.98
CO···CH$_3$OH	-1.32	-0.11	-0.53	2.40	3.492	179.36	OC···CH$_3$OH	-1.65	-0.02	-0.77	2.08	3.664	161.01
CO···CH$_3$-CF$_3$	-1.66	-0.06	-1.07	2.01	3.542	179.56	OC···CH$_3$-CF$_3$	-1.89	0.15	-1.58	-3.15	3.811	179.47
CO···CH$_3$-CCl$_3$	-2.14	-0.04	-1.42	1.57	3.510	179.57	OC···CH$_3$-CCl$_3$	-2.38	0.18	-1.82	1.33	3.735	179.49
CO···CH$_3$-NH$_2$	-1.01	-0.10	-0.36	2.71	3.617	175.10	OC···CH$_3$-NH$_2$	-1.06	-0.09	-0.35	2.65	3.807	143.87

[a] See Eq. 2.

[b] Dipole moment change ($\Delta\mu$) = μ(complex) - $\Sigma\mu$(monomers), where Σ denotes the mathematical sum.

[c] Change in enthalpy (ΔH) = H(complex) - ΣH(monomers), where Σ denotes the mathematical sum, and H denotes the total enthalpy at 298.15.

Table 2: Selected QTAIM properties of the $O\cdots C$ and $C\cdots C$ bonded complexes,[a] obtained using PBE0/6-311++G(d,p). The properties[b] include the charge density (ρ_b/au), the three Hessian eigenvalues of the charge density ($\lambda_{i(i=1-3)}$/au), the Laplacian of the charge density ($\nabla^2\rho_b$/au), the local potential energy density (V_b/au), the local gradient kinetic energy density (G_b/au), the local total energy density ($H_b(= V_b + G_b)$/au), the topological radii of noncovalently bonded atoms (r_a (and r_b)/Å), and the bond path length (r_{bpl}/Å).

Complex[a]	Bond	ρ_b	λ_1	λ_1	λ_3	$\nabla^2\rho_b$	V_b	G_b	H_b	r_a	r_b	r_{bpl}
$CO\cdots CH_3NO_2$	$O5\cdots C1$	0.00268	-0.00125	-0.00097	0.01463	0.01240	-0.00156	0.00233	0.00077	1.686	1.735	3.420
$OC\cdots CH_3NO_2$	$C1\cdots C5$	0.00305	-0.00134	-0.00091	0.01332	0.01107	-0.00133	0.00205	0.00072	1.786	1.882	3.668
$CO\cdots CH_3CN$	$C1\cdots O5$	0.00243	-0.00098	-0.00096	0.01328	0.01134	-0.00140	0.00212	0.00072	1.782	1.704	3.487
$OC\cdots CH_3CN$	$C5\cdots C1$	0.00258	-0.00088	-0.00085	0.01109	0.00936	-0.00111	0.00172	0.00061	1.926	1.797	3.722
$CO\cdots CH_3F$	$C1\cdots O5$	0.00286	-0.00097	-0.00089	0.01614	0.01428	-0.00185	0.00271	0.00086	1.686	1.665	3.351
$OC\cdots CH_3F$	$C5\cdots C1$	0.00337	-0.00094	-0.00089	0.01541	0.01357	-0.00166	0.00253	0.00087	1.845	1.672	3.517
$CO\cdots CH_3Cl$	$O5\cdots C1$	0.00263	-0.00110	-0.00095	0.01421	0.01216	-0.00156	0.00230	0.00074	1.687	1.749	3.436
$OC\cdots CH_3Cl$	$C1\cdots C5$	0.00299	-0.00098	-0.00096	0.01282	0.01088	-0.00134	0.00203	0.00069	1.740	1.884	3.625
$CO\cdots CH_3Br$	$O5\cdots C1$	0.00245	-0.00103	-0.00101	0.01290	0.01085	-0.00140	0.00206	0.00065	1.706	1.775	3.480
$OC\cdots CH_3Br$	$C5\cdots C1$	0.00279	-0.00104	-0.00095	0.01160	0.00962	-0.00120	0.00180	0.00060	1.906	1.772	3.679
$CO\cdots CH_3\text{-}OH$	$C1\cdots O7$	0.00225	-0.00079	-0.00061	0.01248	0.01107	-0.00138	0.00207	0.00070	1.717	1.776	3.493
$CO\cdots CH_3\text{-}OH$	$C1\cdots C5$	0.00268	-0.00103	-0.00040	0.01180	0.01037	-0.00125	0.00192	0.00067	1.785	1.903	3.688
$CO\cdots CH_3\text{-}CF_3$	$C6\cdots O5$	0.00220	-0.00093	-0.00092	0.01179	0.00994	-0.00121	0.00185	0.00064	1.727	1.815	3.542
$OC\cdots CH_3\text{-}CF_3$	$C1\cdots C5$	0.00222	-0.00080	-0.00078	0.00923	0.00765	-0.00091	0.00141	0.00050	1.843	1.968	3.811
$CO\cdots CH_3\text{-}CCl_3$	$O5\cdots C1$	0.00231	-0.00092	-0.00092	0.01249	0.01065	-0.00131	0.00199	0.00067	1.715	1.794	3.510
$OC\cdots CH_3\text{-}CCl_3$	$C5\cdots C1$	0.00251	-0.00085	-0.00084	0.01064	0.00895	-0.00107	0.00165	0.00058	1.932	1.803	3.735
$CO\cdots CH_3\text{-}NH_2$	$O5\cdots C1$	0.00184	-0.00071	-0.00049	0.01001	0.00881	-0.00106	0.00163	0.00057	1.761	1.860	3.621
$OC\cdots CH_3\text{-}NH_2$	$C1\cdots C5$	0.00213	-0.00095	-0.00052	0.00910	0.00763	-0.00092	0.00141	0.00049	2.103	1.955	4.058

[a] See Figures 3 and 4 for the geometrical aspects of $O\cdots C$ and $C\cdots C$ bonded pairs and for atom labeling.

[b] 1 a.u. of charge density (ρ_b) = 6.7483 eÅ^{-3}; 1 a.u. of Hessian eigenvalue of ρ ($\lambda_{i=1,2,3}$) = 24.099 eÅ^{-5}; 1 a.u. of the Laplacian of the charge density ($\nabla^2\rho_b = \lambda_3 + \lambda_2 + \lambda_3$) = $1e\,a_0^{-5}$ = 24.099 eÅ^{-5} = 3.8611×10^{32} C m^{-5}; 1 a.u. of local energy density ($V_b/G_b/H_b$) = 627.5095 kcal mol^{-1}; topological radii and bond path lengths (r's) are in Å. See text for more detail.

Table 3: The changes in the normal mode vibrational stretching frequencies ($\Delta\omega$/cm^{-1}), in the bond distances (Δr(CO)/Å), and in the infrared intensities (ΔI/km mol^{-1}) associated with the CO bond for the O···C and C···C bonded complexes, obtained using PBE0/6-311++G(d,p).[a,b]

Complex[b]	$\Delta\omega$[c]	Δr(OC)[d]	ΔI[e]	Complex[f]	$\Delta\omega$[c]	Δr(CO)[d]	ΔI[e]
CO···CH$_3$NO$_2$	-8.2	0.00093	8.4	OC···CH$_3$NO$_2$	6.8	-0.00099	22.8
CO···CH$_3$CN	-7.1	0.00080	6.7	OC···CH$_3$CN	9.7	-0.00081	22.8
CO···CH$_3$F	-5.3	0.00059	5.5	OC···CH$_3$F	6.1	-0.00065	14.2
CO···CH$_3$Cl	-5.2	0.00056	4.8	OC···CH$_3$Cl	11.6	-0.0006	19.6
CO···CH$_3$Br	-5.2	0.00054	4.5	OC···CH$_3$Br	14.3	-0.00056	22.3
CO···CH$_3$OH	-2.7	0.00027	2.0	OC···CH$_3$OH	9.5	-0.00027	12.2
CO···CH$_3$-CF$_3$	-5.4	0.00060	4.8	OC···CH$_3$-CF$_3$	6.6	-0.00059	16.2
CO···CH$_3$-CCl$_3$	-5.0	0.00054	4.4	OC···CH$_3$-CCl$_3$	14.6	-0.00054	23.4
CO···CH$_3$-NH$_2$	-1.4	0.00010	0.0	OC···CH$_3$-NH$_2$	8.8	-0.00099	11.6

[a] The changes are given relative to isolated species. The corresponding ω, r, and I values for isolated CO in its $^1\Sigma$ electronic ground state are ca. 1.1260 (1.1282 Å), 2241.2 (2170 cm^{-1}), and 93.4 km mol^{-1}, respectively, where parentheses indicate the experimental values.[63]

[b] See Figure 3 for the geometric details of the O···C bonded pairs.

[c] $\Delta\omega$ = ω(complex) - ω(free).

[d] Δr = r(CO distance in complex) - r(CO distance in monomer).

[e] ΔI = I(complex) - I(free).

[f] See Figure 4 for geometric details of the C···C bonded pairs.